3.1 Bericht Teilprojekt 8

3.1.1 Titel / Title

Gasphasen-Kondensation von Kohlenstoff-Nanopartikeln und ihre strukturelle Charakterisierung

Gas phase condensation of carbon nanoparticles and their structural characterization

3.1.2 Berichtszeitraum / reported period

01.07.2003 - 30.06.2006

3.1.3 Projektleiter / priniciple investigator

Mutschke, Harald, Dr. rer. nat.,
Friedrich-Schiller-Universität Jena

3.2 Zusammenfassung / Abstract

3.2.1 Wortlaut des Antrags / abstract of the proposal

In der Fortsetzung dieses Projektes werden wir uns zum ersten weiter mit den Auswirkungen des Einbaus von Heteroatomen in Kohlenstoff-Nanopartikel befassen. Zweitens soll der Einfluss von Nukleations-Keimen auf die Kondensationsprozesse untersucht werden. Zum dritten ist geplant, die Möglichkeiten zur Nukleation von Nanodiamanten in den verfügbaren Syntheseprozessen zu studieren. Die Kondensationsprozesse sowie die resultierende Mikrostruktur und optische Eigenschaften der Partikel sollen detailliert untersucht werden, um das Verständnis für die Eigenschaften analoger kosmischer Nanoteilchen zu verbessern.

The continuation of this project is aimed in the investigation of (1) the effect of hetero-atom incorporation into carbon nanoparticles, (2) the influence of nucleation seeds on carbon condensation, and (3) the possibilities for nucleation of nano-diamond structures. The condensation processes and the resulting microstructure as well as the optical properties of the particles will be studied in detail in order to improve our understanding of analogous cosmic nanoparticles.

3.2.2 Zusammenfassung des Berichts / abstract of the report

In this project, we have investigated the formation of carbonaceous nanoparticles by means of condensation experiments in connection with electron microscopic and spectroscopic techniques. This comprises investigation of (1) the incorporation of hydrogen in order to set constraints for the carrier of the interstellar 3.4 μm band, (2) the influence of carbide nucleation seeds on the condensation process, and (3) the influence of an aromatic precursor molecule on the properties of the condensate. Products from a variety of processes such as laser pyrolysis with pulsed and continuous-wave lasers, laser ablation in reaction gas atmospheres, and combustion at variable C/O ratio have been applied. Analytical techniques included spectroscopic measurements from the infrared to the far-ultraviolet wavelength range. In the former, measurements have been carried out in-situ to avoid contamination with atmospheric hydrocarbons. In the latter, special emphasis was given to the separation of scattering and absorption losses.

The most pronounced differences in the structure and the spectroscopic properties of the condensates have been found to be related to variations in the reaction temperature. Pulsed processes such as laser ablation and pulsed-laser pyrolysis involved high temperatures and fullerene-like condensates are produced. The influence of nucleation seeds has been found to be minor, the one of an aromatic precursor was significant but did not change the structures dramatic. In contrast, cw laser pyrolysis and combustion at low C/O ratio produce different structures and a large amount of volatile components under certain conditions. The structures have been explored in detail by high-resolution electron microscopy and conclusions for the nucleation processes at high temperatures have been drawn. The infrared and UV spectra measured on the condensates have been compared to astronomical spectra mainly of evolved objects. Condensates rich in volatiles possess spectral features partly in common with condensates in such astrophysical environments shedding light on the relation of amorphous carbon grains and aromatic molecules in space. The strong UV resonance of such materials is similar to the interstellar UV hump but at a slightly different position.

During the project, a close connection to TP 11 has been developed. Carbonaceous materials produced in low-temperature pyrolysis and combustion processes are interesting sources of aromatic molecules for spectroscopic studies. Extraction of the aromatics and analysis by mass spectrometry and gas chromatography has revealed their molecular composition.

3.3 Ausgangsfragen, neuster Stand der Forschung / Initial goals, current status of the field

Carbonaceous nanoparticles are an abundant and important component of the interstellar medium and of circumstellar disks and outflows. Spectral signatures of these dust particles and of related species such as large aromatic molecules are found in the interstellar extinction as well as in emission from young stellar objects and from galaxies. However, the assignment of these features to corresponding carbon structures is difficult, since carbon modifications and structures are extremely variable and the available experimental data on the relation of optical and structural properties of carbon structures are not sufficient yet. For instance, it is not clear whether the interstellar particles producing the interstellar 3.4 μm absorption band and identified as consisting of a hydrocarbon material poor in oxygen and nitrogen and containing both aromatic and aliphatic carbon forms (Pendleton and Allamandola 2002) are also related to the 217.5 nm UV interstellar extinction feature, which may represent a π-electron transition band of aromatic carbon structures.

Moreover, the carriers of the "aromatic infrared emission bands", which are ubiquitous in interstellar and circumstellar galactic and extragalactic environments (e.g. Kwok *et al.* 2001, Peeters *et al.* 2002), have not yet been firmly identified, although it is clear that they have to be small aromatic structures with the size of nanoparticles or large molecules. In principle, these characteristics are similar to those required for the carrier of the UV extinction feature (Duley and Seahra 1999) and evidence for spectral features similar to the interstellar band is available (e.g. Duley and Lazarev 2004), however, currently the idea of onion-like graphitic grains is more popular (Chhowalla *et al.* 2003, Iglesias-Groth 2004, Tomita 2004). In a few objects in space, preferentially the environments of young stars, diamond grains have been identified by assignment of C-H stretching bands observed at 3.43 and 3.53 μm (Van Kerckhoven *et al.* 2002).

To improve our understanding of carbonaceous nanoparticles in space therefore means, on the one hand, to establish firm relations between carbon structures and spectroscopic signatures and, on the other hand to study the relation of molecular and solid species in formation processes. Unfortunately, the chemical networks determining the formation routes of nanoparticles from the gas phase are quite complex, even in "well-defined" laboratory systems. Therefore, our current knowledge about the condensation and modification of carbonaceous nanoparticles is still limited. A scenario for graphite grain condensation within the O-rich CO core of Type II supernovae has been proposed by Clayton *et al.* (2001). The authors claimed the formation of C_n linear chains which can be transformed into ringed isomers, the building blocks of bigger carbon structures. The most probable places for the formation of PAHs are the circumstellar envelopes of carbon-rich late type stars (Allain *et al.* 1997). The formation process of interstellar PAHs has not been clarified so far. One possibility is that PAHs are precursors, intermediate steps or side products in the carbon nanoparticle condensation in different astronomical environments and therefore their composition should be closely related to the condensation process. From laboratory soot condensation experiments it is quite evident that soluble components are formed in addition to soot during the condensation process (Keller *et al.* 2000). Better laboratory data on these processes as well as on the spectroscopic properties of the resulting materials are urgently needed for the interpretation of the observations (Reynaud *et al.* 2001).

3.4 Angewandte Methoden / Experimental methods

3.4.1 Laser ablation

The laser ablation experiment uses a pulsed laser Nd:YAG laser working at 532 nm (pulse length 5ns, pulse energy 230mJ) for evaporation of solid carbon material. The condensation of carbon particles is caused by collisions between the generated C-clusters (Witanachchi *et al.* 2000) and cooling gas atoms. We have applied helium, hydrogen, water vapor and mixtures of those as reactive and cooling gases. In order to influence *the size* of the originally condensed particles and the amount of *hydrogen* that can be incorporated into the carbon structure, the pressure in the reaction chamber was varied between 1and 10 Torr and the laser power densities in the focused laser beam was varied between $2x10^8$ and $9x10^9$ W/cm^2. In most experiments graphite targets have been used. In two other experimental series the *co-condensation* of graphite / titanium carbide and graphite / silicon carbide targets has been studied.

The laser ablation source has been combined with a molecular beam technique in order to deposit the soot particles onto an optical window, transparent for different spectral ranges (FUV/UV/VIS and NIR/MIR), and to measure their infrared spectral properties *in situ*. In the second project phase, the setup for laser ablation has been extended with a substrate mount that can be *heated* to temperatures of up to 600K which allowed studying

the influence of adsorption of organic gas-phase molecules on the reactive surface of nano-sized carbon grains. The physical adsorption of such molecules could be observed by in-situ measurements of the 3.4μm C-H stretching band strength. The adsorbed molecules were easily desorbed from the particle surfaces by heating the condensed material up to 273K.

3.4.2 Laser-induced gas pyrolysis

In this term of the project the laser pyrolysis technique capabilities have been further developed. The incorporation of an URENCO-TEA-CO_2 laser (Modell ML104 produced by Uranit) with a maximum output energy of 6 J and a working frequency between 10 and 50 Hz into the pyrolysis setup has provided the necessary tool for studying the properties of the pyrolysis products in dependence on the *laser power*. The use of ethylene and benzene precursor gases has allowed us to investigate the influence of higher hydrogen content than with the previously used acetylene and of an *aromatic precursor* structure on the pyrolysis products. In addition, thermal *annealing* of some of the samples has been performed in order to understand the incorporation of volatile species into the grains during the condensation processes.

3.4.3 Combustion (CAST)

The Combustion Aerosol Standard generator (CAST, Jing-CAST Technologies) is a device used for generation of "standard" soot particles with controllable properties. For this purpose it uses condensation in a co-flow diffusion flame of propane and air at variable flow rates. The combustion products are extracted from the flame and quenched by a strong flow of cool N_2 intersecting at a certain flame height. The quenching prevents the soot particles from further oxidation, thermal processing, deposition and agglomeration. The main parameter determining the soot condensation is the *C/O atomic ratio in the flame* which is inversely correlated with the flame temperature. We have used C/O ratios between 0.29 and 0.61. The condensates have been deposited to CaF_2 optical windows, TEM grids and aluminum foil by means of an impactor with rotating stages (Hauke, model LPI ROT 25/0.018/2.0), the stage numbers corresponding to increasing aerodynamic diameter cutoffs (between 0.0180 and 16.0 μm for stages 1 to 11, respectively).

From the particles deposited on the aluminum foils, the deposited masses at the different stages have been determined by vaporization/combustion and subsequent CO_2 detection. In this analysis, the components released by vaporization at T<350°C (OC1) and T<650°C (OC2, "organic carbon") could be measured separately from the remaining "elemental carbon" (EC) component. Samples deposited by the first stage of the impactor, i.e. the smallest-size component, tended to possess the highest amount of OC. Thermal treatment up to 650°C has also been performed on the samples deposited to optical windows for separation of the absorption contribution of the volatile components. These experiments have been performed in collaboration with Dr. M. Schnaiter from the Institut für Meteorologie und Klimaforschung Karlsruhe.

3.4.4 Spectroscopic and TEM analysis

The analysis of the samples includes spectroscopy in a wide wavenumber range from the mid-infrared (MIR) to the far-ultraviolet (FUV). In this project period, the UV measurements have been extended by using an integrating sphere accessory to the Perkin Elmer Lambda 19 spectrometer and by angle-resolved light-scattering measurements with the FUV spectrometer. This allowed separate measurements of the scattering and absorption contributions to the extinction spectra, which provides very important information in order to correctly characterize the deposited products. For comparison, absorption and scattering curves have been calculated from published optical constants of carbonaceous materials (Zubko *et al.* 1996 and Schnaiter *et al.* 1998) for single and aggregated particles.

Particle sizes and structures of the condensed carbon grains have been determined by means of transmission electron microscopy at both low (TEM) and high resolution (HRTEM, 300 keV). The HRTEM is equipped by an energy dispersive X-ray analysis system (EDX) for quantitative analysis of the chemical composition. The vapor-phase condensed particles were mostly directly deposited on Lacey carbon supported TEM grids. HRTEM provides a direct view inside the medium-size order of the carbon structures by imaging the edge-on aromatic layers. In carbon nanoparticles, graphene layers can curl within the particles but they still appear as fringes. For derivation of quantitative information about the carbon structures we performed image analyses similar to Palotas *et al.* (1996) and Galvez et al (2002). Moreover, we constituted a new possibility to get structural information on very disordered systems. The HRTEM bright field micrographs were Fourier transformed to see 'periodicity' in the structure and to derive main distances between the observed graphene layers. The corresponding FT images show rather broad arcs with a distribution of different radii. We have used the intensity profiles of the computer-generated diffractograms to measure the mean distances d_{002} between the

graphene layers for the chosen sample area. The mean L_a sizes of these graphene layers were determined by selecting an adequate sample area of a diameter of 15 nm for all evaluated HRTEM images. These image parts were skeletonized by filtering the images using ring-shaped masks, which were evaluated to eliminate the majority of periodicities without physical sense. An inverse FT from the filtered image was used to generate the skeletonized image which was employed to measure the sizes of the graphene layers. To avoid artifacts the filtered images were carefully compared to the raw images of the sample area. The quantitative analyses using FT of the digital images and measurements of graphene layer lengths and distances were performed by applying the Digital Micrograph 3.9.0 software. The image analyses have been employed to condensed carbon from laser pyrolysis and laser ablation.

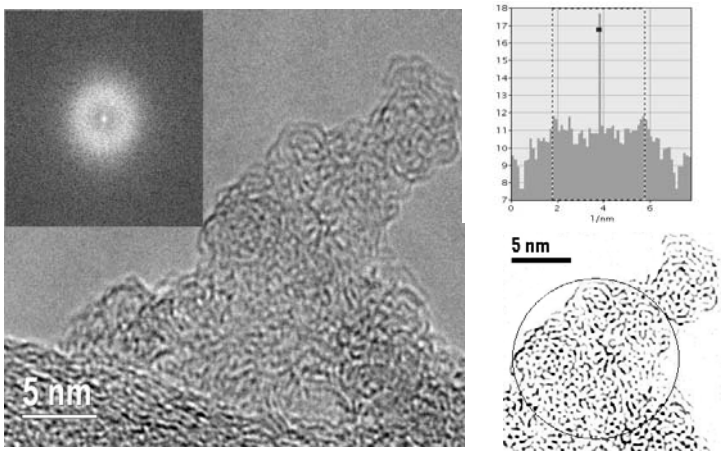

Fig. 1:. Bright field HRTEM image of gas-phase condensed soot grains. The insert shows the Fourier transformed image. The right upper panel shows the intensity profile of the FFT image whereas the right lower panel represents a skeletonized image of the left micrograph.

3.5 Ergebnisse und ihre Bedeutung / Results and their importance

3.5.1 Hydrogen incorporation by laser ablation in reactive atmosphere

In our study of gas-phase condensation of carbon grains we have focused on the relation between the internal structure of the condensed carbon grains and its effect on the spectral properties of the grains. For the spectroscopy the main activities were concentrated on the optimization of hydrogen incorporation into the soot structure and its influence on the spectral properties from FUV to the IR range. The incorporation of hydrogen into carbon structures can take place in two different ways. Firstly, it could be bonded to aromatic sp^2 or to saturated sp^3 hybridized carbon atoms. In both cases hydrogen strongly affects the structure and spectroscopic properties of the generated soot particles. For an efficient integration of these atoms we have varied the temperature in the condensation zone and used new reactive gas mixtures such as He/H_2O for quenching and condensation of carbon nanoparticles. The sizes, the morphological appearance and the internal structure of soot grains produced in the laser ablation experiments using a pulsed laser did not show strong variations as shown in Fig. 2. In both cases very small fullerene-like carbon grains are visible. The left panel shows carbon grains containing a low H/C ratio of 0.14 and the carbon grains in the right panel are typical for materials with high H/C ratio of 0.5. The grain sizes and the strongly bent graphene layers are comparable. The difference is the lower order of the grain structures in the right image.

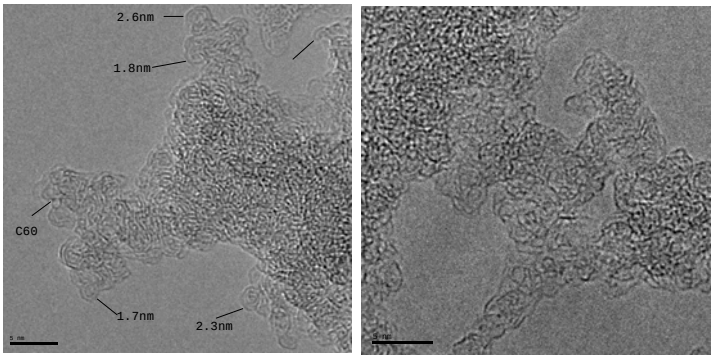

Fig. 2:. HRTEM bright field images of carbon grains with low (left panel) and high hydrogen content (right panel). In both images very small seed-like particles with fullerene structures are visible.

Table 1 shows an overview on the compositional and structural properties of the carbon grains produced in He/H_2 atmospheres at different pressures. There are strong variations in the hydrogen content but much smaller differences in the mean graphene layer sizes and distances between the graphene layers. The content of sp^2 hybridized carbon was found to be 57% in a low-hydrogen containing sample (H/C=0.16) and 48% in a sample with a H/C ratio of 0.5. The content of sp^2 hybridized carbon was measured using EEL spectroscopy of free-standing grains. However, despite only small structural varieties occurred, strong differences were found in the spectral properties of the condensed carbon matter. Fig. 3 contains the IR and FUV spectra of the carbon material presented in Table 1.

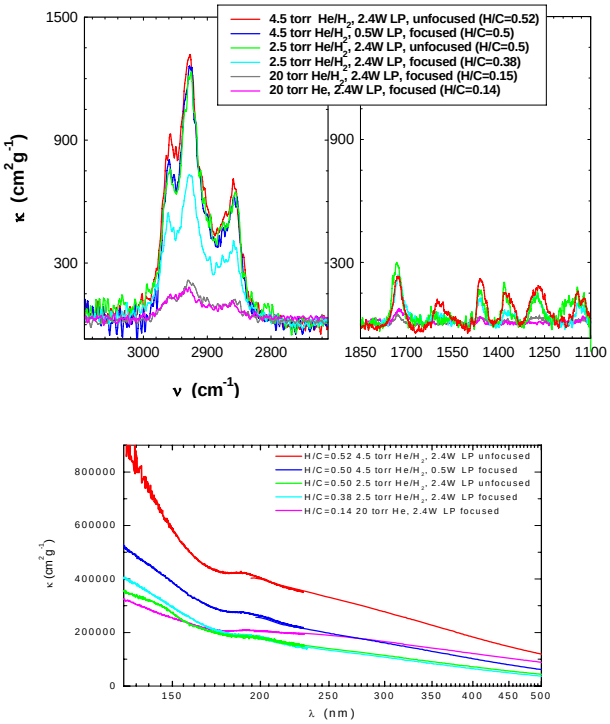

Fig. 3: IR and FUV/UV/VIS spectra of condensed soot grains containing different H/C ratios. The samples are the same as reported in Tab 1.

The incorporated hydrogen is mainly bonded to sp^3 hybridized carbon atoms forming up methyl ($-CH_3$) and ethyl ($-CH_2$) groups showing strong absorption bands in the 3.4 µm (2800-3000 cm^{-1}) range of the IR spectrum due to stretching vibrations. Maximum mass extinction coefficients of 1500 cm^2g^{-1} at 3.4 µm for the laser ablated materials could be measured. These saturated, aliphatic functional groups are bonded to the aromatic islands or connect the strongly bent graphene layers in the particles. The mean sizes L_a of the aromatic graphene layers are rather small in the fullerene-like grains comprising no more than 3 condensed rings in the L_a extension. The insertion of hydrogen in the condensing grains is highest for samples produced with low laser

power or unfocused laser beam. An explanation for this specific result could be found in the condensation mechanism and rate coefficients of the chemical equilibrium between hydrogen abstraction and C-H bond formation.

LP (W)	P (Torr)	Gas	Mean seed size (nm)	Mean L_a size (nm)	Mean d_{002} value (nm)	H/C
2.4f	20	He	1.56	0.53-0.6	0.43	0.14
2.4f	20	He/H_2 2:1	1.42	0.488	0.51	0.16
2.4f	2.5	He/H_2 2:1	1.2	0.45	0.54	0.39
0.5f	4.5	He/H_2 2:1		0.42	0.59	0.5
2.4uf	4.5	He/H_2 2:1	1.43	0.42	0.57	0.52

Table 1: Structural parameters of soot grains containing different H/C ratios.

The complete IR spectrum shows the same bands that can be observed in the spectrum of carbon particles condensed in He/H_2O atmospheres. The incorporation of hydrogen in condensing carbon grains using He/H_2O atmospheres was however much more efficient compared to the samples produced in He/H_2 atmospheres. The mass extinction coefficients at 3.4 µm vary between 300 and 1500 cm^2g^{-1}. We produced a carbon sample with the highest H/C ratio of 0.54 in a He atmosphere with a partial pressure of 0.09 Torr H_2O. Typical for all IR spectra of the laser ablation soot samples is the occurrence of vibrational bands at 3300 and 2100 cm^{-1} caused by C-H and C-C groups of sp hybridized carbon atoms. These bands disappear when the samples are exposed to air. The observed instability of the IR bands due to triply bonded carbon is typical for polyynes (Bogana *et al.* 2005). A much more detailed description of the results of the laser ablation experiments can be found in Jäger *et al.* (2007b).

The FUV/UV/VIS spectra of all samples (see lower panel in Fig. 3) did not show distinct UV bumps but a strong rise of the mass absorption coefficient up to the expected electronic σ–σ* transition at wavelengths less than 100 nm. The very small peak at about 190 nm is not caused by π–π* transitions but by electronic transitions in C=O groups which can also be find in such carbon structures. The very broad distribution of the electronic π–π* transitions that are partially masked by the strong absorption in the FUV are due to the strongly varying curvatures of the graphene layers in the fullerene-like nano-sized carbon grains.

The absorption properties of soot particles containing an H/C ratio of 0.5 reproduce the intensity as well as the spectral profile of the interstellar 3.4 µm absorption band (see Fig. 4). However, the 80 ppm interstellar carbon available to form solid grains is completely consumed in order to reproduce the high intensity of the interstellar band.

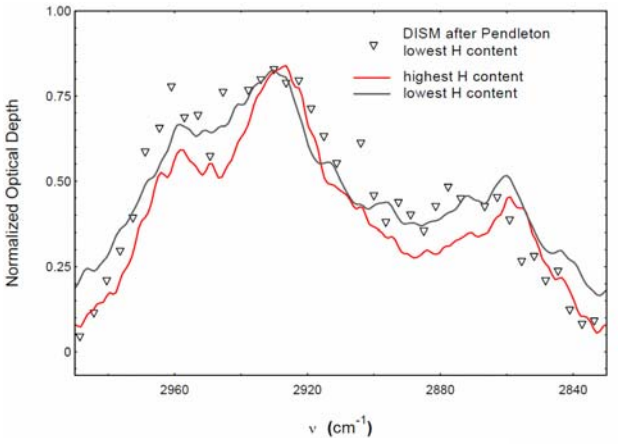

Fig. 4: Interstellar absorption 3.4 µm absorption profile compared to a lab materials with high H content and a $\kappa(2950cm^{-1})=1400cm^2g^{-1}$ (corresponding H/C ratio of 0.5) and low H content (H/C=0.14). In order to fit the intensity of the DISM profile one needs about all the left carbon (80 ppM).

The effect of physically adsorbed organic molecules has also been investigated by in-situ IR spectroscopy. We found a very efficient adsorption of molecules from the gas phase within seconds in air, and within a few hours (2-3) in vacuum (10^{-6} mbar). The increase of the mass extinction coefficient of the C-H

stretching vibrations was especially strong for the small fullerene-like carbon grains due to their large surface. The enhancement of the C-H bands is coupled with an increase of the –C=O band at about 1720 cm^{-1}. A certain amount of the increase results from the reaction of the soot surface with water molecules leading to the formation of C-H bonds on the surfaces. Heating of the sample to 500 K results in the abstraction of the physically bonded alkyl groups. After hydrogen abstraction the original mass extinction coefficient is obtained. The results of the adsorption experiments demonstrate that for carbon samples containing small and strongly disordered particles only in-situ IR measurements provide real mass extinction coefficients in the region of the stretching vibrations of alkyl groups at 3.4 µm.

3.5.2 Co-condensation of graphite and carbide grains

We have studied the influence of carbides on the nucleation process of carbon grains. The experiments were performed by laser ablation of mixed targets (graphite/carbide mixtures) in different quenching gas atmospheres. The precondensed carbide can serve as nucleation seeds for further condensation of carbon materials. Such nucleation seeds of titanium carbide could be identified in meteoritic graphite grains by Stadermann et al (2005). Their sizes range from 15 to 500 nm. Lodders and Fegley (1999) have calculated condensation sequences of dust grains in N-type stars (C/O>1) and found that TiC is the first condensate in the shells of such stars. SiC usually condenses after graphite but there are exceptions caused by temperature differences between gas and grains (Chigai and Yamamoto 2003).

Under such conditions SiC grains can either precede the graphite condensation or can be formed simultaneously with graphite grains. Therefore, we were interested in the study of the influence of titanium carbide and silicon carbide on the gas-phase nucleation process of carbon grains. The analytical characterization of the generated carbon nanopowders was mainly based on high-resolution electron microscopy combined with EDX analyses. The optical properties of the generated carbon samples were studied by means of FUV, UV/VIS and IR spectroscopy.

The result of these studies can be summarized as following. The influence of titanium carbide and silicon carbide on the structure of the condensing carbon grains is negligible. In the case of TiC we were able to identify cubic TiC crystals up to sizes up to 25 nm but also small amounts of titanium oxide and metallic titanium.. This result was based on the EDX analysis of the individual grains. The TiC crystal structure was identified by measuring the distances between the lattice fringes which were visible in the HRTEM images. These grains are covered by a small amorphous carbon layer. However, the majority of the condensates show the same very small fullerene-like carbon grains as already observed in the pure graphite samples. Hence, the effect of the spectral properties of the grains is rather low. The hydrogen insertion into the carbon structures is comparable to the samples prepared with the pure graphite target under the same conditions. The maximum mass extinction coefficients for the 3.4 µm stretching region are nearly similar. The spectral properties in the FUV/UV/VIS region are caused carbon structures which are completely comparable to to structures produced with pure graphite.

A difference in the condensation was found for samples produced by laser ablation of mixed graphite/SiC targets. HRTEM images did not show distinct SiC particles but also the fullerene-like particles very small carbon seeds. However, EDX analyses have shown that at least up to 4% SiC was incorporated in the carbon structure (see Fig. 5). The structural properties of the condensed carbon seeds is again the same like in the laser ablation of pure graphite targets.

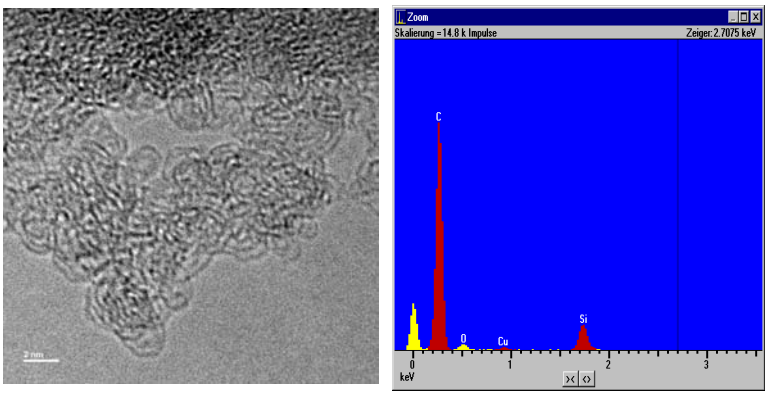

Fig. 5: HRTEM image of carbon grains produced by co-condensation of graphite and SiC. The very small seed-like grains show fullerene-like structures. The right panel displays the EDX analysis of a representative area of the sample. An amount of 6 % Si is contained in the carbon material.

The spectral behaviour of these SiC containing samples is again affected by the fullerene-like structures of the small-sized condensed soot grains. The fullerene-like structures with strongly bent graphene layers and very disordered structure show the same IR spectral properties and typical FUV/UV/VIS behaviour all the soot samples produced by our laser ablation experiments.

3.5.3 Influence of precursor gas and laser power on laser pyrolysis products

In our study of particle condensation by laser induced pyrolysis of hydrocarbon gases, the use of precursors with different bonding nature (aromatic/aliphatic), such as benzene, acetylene and ethylene has provided important information about the incorporation of aromatic molecules into the grains as well as about the influence of the precursor gas on the morphology and internal structure of the particles. The incorporation of hydrogen into the grains has been studied by using ethylene as precursor instead of acetylene. Systematic studies concerning the effect of the different experimental parameters on the final properties of the products have been also extended. In previous studies, the influence of the catalyst/precursor ratio was investigated in detail (Llamas Jansa 2002, Llamas Jansa *et al.* 2003), but no investigations of the laser power effect were possible at that time.

a) Size, morphology and internal structure

TEM and HRTEM images show that the pyrolysis particles are rather spherical in shape and that they easily form aggregates containing hundreds to thousands of particles. The size of the particles ranges from 3 to 14 nm and shows a dependence on the nature of the precursor, with larger particles seen in the benzene-based samples. An inverse correlation between the laser power and the size of the particles is observed. The internal structure of the particles is made of coagulation seeds with sizes between 3 and 5 nm that are probably the beginning of further graphitization of the grains into more onion-like structures. The amount of these seeds is related to the precursor gas, with a higher density of seeds in the benzene-based samples. The internal structure of the seeds is made of BSUs (Robertson and O'Reilly 1987) that can be formed of more or less extended graphene layers. No correlation between the size of the graphene layers and the precursor or the laser power is found. Particles made of an organic component similar to that observed in the CAST samples (see 3.5.4.) and different from the more refractory ones have been observed in some of the benzene-based samples. The organic component has been further studied by means of thermal treatments.

b) Spectroscopy

The results of the infrared spectroscopy show that the incorporation of aromatic groups is highly effective for the benzene precursor compared to the processes based on aliphatic precursors (Fig. 6). This fact is seen by the appearance of a strong "solo" aromatic C-H out-of-plane bending band at ~885μm^{-1}, which is not present in the acetylene and ethylene samples. The presence of the solo band together with the other aromatic deformation bands at wavenumbers between 885 and 755 cm^{-1} is similar to the observed profile in the combustion CAST samples. A further incorporation of hydrogen atoms due to the use of ethylene instead of acetylene for the pyrolysis is not seen in the IR results. This observation indicates that, although the condensation mechanism may have been changed with ethylene, the hydrogen has been likely released in the form of H_2 molecules during the process and is not incorporated into the grains.

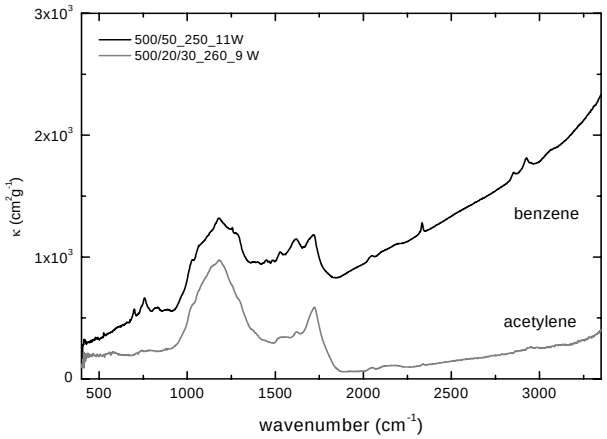

Fig. 6: Infrared spectral curves corresponding to pyrolysis samples produced with different precursors. The legend indicates the experimental parameters: gas flow ratio, pressure and laser power, respectively.

Systematic studies of the spectral properties in the wide wavenumber range from the near infrared (NIR) to the far ultraviolet (FUV) have been carried out for all the series of samples produced. The results show that no correlation between the laser power and the optical behaviour of the samples can be drawn but that the nature of the precursor gas strongly influences the spectral properties (Fig. 7). The curves have been characterized using deconvolution into Gaussians (parameters peak position, width and area) and by the gap energy (E_g) parameter derived from the Tauc's relation. A shift of the main absorption peak towards smaller wavenumbers and a decrease of the E_g value have been observed for the samples produced with benzene compared to the aliphatic-based samples.

For this analysis it has been important to separate the scattering contribution, especially at the small wavenumbers close to the optical gap. The experimental investigation of the scattering coefficient showed that the benzene-based samples present considerably higher scattering in the ~1-4 μm-1 range with values between 51 and 56% at 4 μm^{-1} and between 65 and 79% at 2 μm^{-1} than the acetylene samples with 27 and 47 % at 4 μm^{-1} and between 11 and 38 % at 2 μm^{-1}. This fact is likely related to the smaller particles observed for the latter samples.

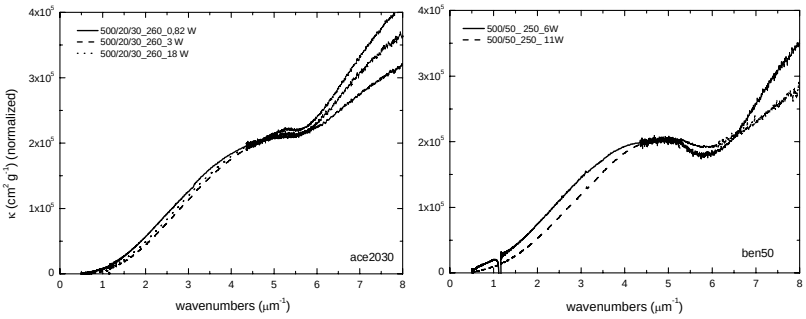

Fig. 7: UV/VIS spectral extinction curves for samples produced with acetylene (left panel) and benzene (right panel).

Scattering measurements carried out in the FUV range demonstrate that the strong rise of the FUV extinction towards higher wavenumbers seen in the spectral behaviour of the pyrolysis samples is not a scattering feature but a characteristic of the absorption. Simulated curves obtained using optical constants of carbonaceous materials from the literature (Zubko *et al.* 1998 and Schnaiter *et al.* 1998) do fit the measurements to a certain extent when considering particle aggregates. The simulations show that for $\lambda^{-1} > 4$ μm^{-1} the scattering curve is generally structured and nonlinear, but does not strongly increase. To our knowledge these are the first scattering measurements on soot particles at far UV wavelengths.

c) Thermal annealing

Thermal annealing experiments of some of the pyrolysis samples have been carried out in the 350-450°C range in vacuum in order to collect more information about the presence of volatile components in the pyrolysis samples (see also 3.5.4). The results show that the 5.1 μm^{-1} feature present in the UV spectra of some of the samples disappears after the thermal treatment. Second, a shift of the main absorption peak occurs with increasing annealing temperature. Additional information provided by IR spectroscopy concerns the loss of oxygen-based components (C=O bands) and a decrease of the content of aromatic groups in the benzene-based samples. These observations indicate that the 5.1 μm^{-1} feature is likely related to the presence of oxygen on the particles probably incorporated during the condensation processes. The fact that the aromatic groups are diminished at these temperatures also indicates that they are caused by some kind of PAHs representing part of the volatile component of the grains.

3.5.4 Spectroscopic properties of soot rich in volatiles

a) Combustion (CAST) products

Whereas the pulsed-laser induced processes used in our laboratory generally produce amorphous-carbon condensates through processes which strongly limit the formation of a volatile, i.e. molecular component, we have obtained condensates rich in such molecules through collaborations. In the NILPRP Bucharest (collaboration with I. Voicu), cw-laser-induced gas pyrolysis has been applied to produce carbonaceous condensates containing up to 30% of aromatic molecules. These products could be obtained in large amounts allowing the chemical analysis of the molecular component. In the IMK Karlsruhe (with M. Schnaiter), standard (CAST) soots have been produced by combustion of propane at C/O atomic ratios between 0.29 and 0.61, which have been investigated mainly by spectroscopic and electron microscopic techniques. The amount of volatiles (the „organic component, OC“) has been measured by a heating experiment and correlates with the C/O ratio (see 3.4.2.).

For the infrared (IR) spectroscopic investigation, material originally deposited on aluminum foils has been embedded into KBr pellets. The spectra of samples produced at high C/O ratios differ from those produced at low C/O ratios first by a much lower IR continuum absorptivity (a factor of six for C/O=0.5 compared to C/O=0.29) and second by the presence of strong aromatic C-H bands such as the stretching band at about 2950 cm^{-1} and the out-of-plane bending vibration bands in the 700-900 cm^{-1} range (see Fig. 8). These bands are absent in the condensate produced at C/O=0.29. The out-of-plane bending vibrations at the lowest wavenumbers indicate highly hydrogenated aromatic rings, which are greatly diminished after heating to 350°C. This leads to the conclusion that the volatile component is dominated by relatively small polyaromatic molecules which form an abundant component of the condensates (OC content up to 65%).

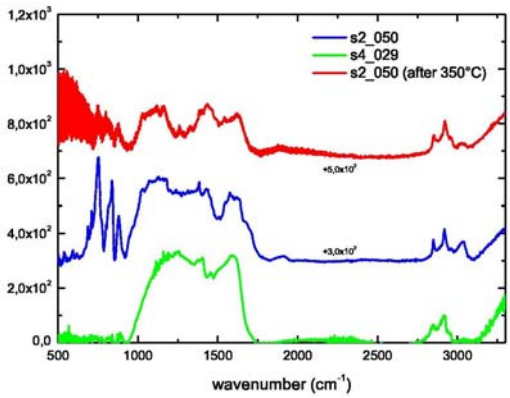

Fig. 8: Infrared absorption spectra (continuum subtracted) for CAST soot produced at C/O=0.29 (lower curve) and C/O=0.50 (middle) as well as the C/O=0.50 material after annealing at 350°C. Note the varying strength of the aromatic C-H bands at wavenumbers <1000 cm^{-1} and >3000 cm^{-1}.

Correspondingly, electron microscopy revealed that condensates obtained at high C/O ratio do not consist of well isolated soot particles with graphitic structure (such as those produced at low C/O), but appear covered with or even consist of a structureless amorphous material which may be dominated by aggregated molecules. At intermediate C/O the graphitic soot particles and the structureless molecular component are even seen as separate populations, the latter forming rather large spherical particles (see Fig. 9). The correlation between the presence of this structureless component and the strength of the aromatic C-H bands indicates that the polyaromatic molecules formed in the combustion tend to condense either as a separate population of particles or, at the highest C/O ratios and lowest temperatures, dominate the condensed material as a whole.

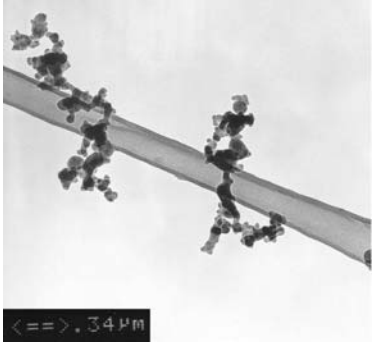

Fig. 9: TEM image of a CAST soot produced at C/O=0.4 showing larger spherical particles of a condensed molecular component attached to aggregates of smaller refractory particles.

These changes of the chemical and structural properties of the condensates are reflected by the UV spectra of the samplesl. The dependence on the C/O ratio is especially pronounced for the smallest size fraction deposited with the impactor on CaF_2 substrates (Fig. 10a). At low OC content the π-electron transition band of the material is peaking at about 3.5 μm^{-1} and extends down to 0 μm^{-1}. For C/O=0.5 it narrows considerably and shifts its peak to about 4.8 μm^{-1}. The optical gap energy determined from the slope of the absorption at visible wavelengths increases to values of about 1.7 eV. The absorption in the visible lowers by about one order of magnitude and obtains much steeper wavelength dependence (Schnaiter *et al.* 2006). At near infrared wavelengths scattering becomes dominant over absorption and gains also a higher importance in the ultraviolet (albedo up to 0.4, Fig. 10b) because of the influence of the larger particle size (I. Llamas Jansa, PhD thesis 2006).

The spectroscopic and TEM investigation after thermal treatment at 450°C supports these findings on the influence of molecular aggregates. The loss of the OC component leads to distinctive changes in strength, width and peak position of the π-electron band (Fig. 10c), which can be interpreted as the evaporation of part of the volatiles plus a carbonization of another part, which is clearly indicated by an increase of the absorption at wavenumbers between 0.5 and 2.5 μm^{-1}. The spectra of CAST soots produced at C/O=0.29 lack these annealing effects. With the measurements in the FUV it was possible for the first time to explain the reasons for the OC dependence of the albedo and the visible absorption in terms of the changes of the π-electron transition band profile.

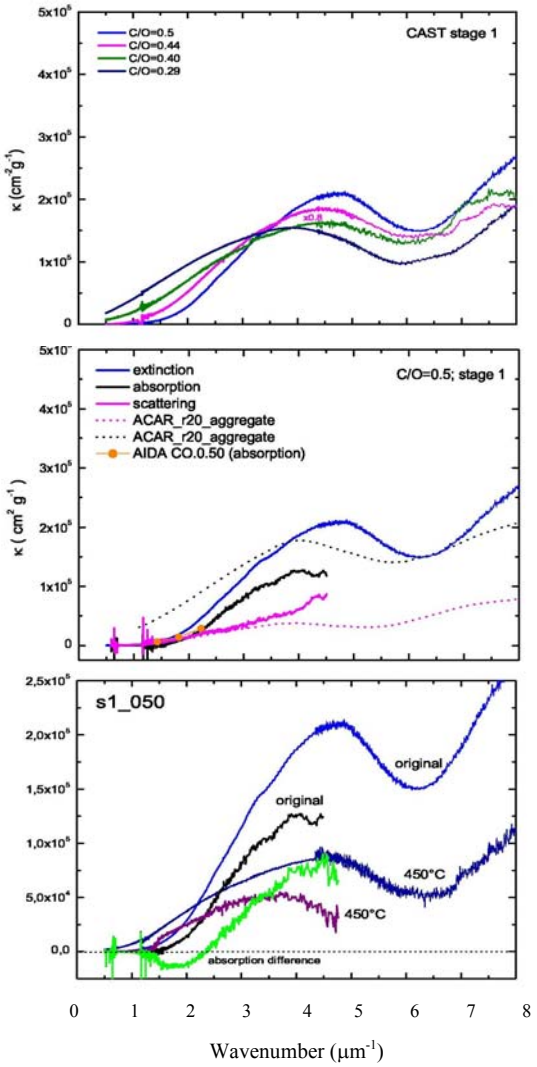

Fig. 10: UV spectra of CAST soots produced at different C/O ratios (top, a), contributions of absorption and scattering to the extinction for C/O=0.5 (middle, b, dotted line is a simulation) and change in extinction and absorption after annealing at 450°C (bottom, c, green curve is the difference of the absorption spectra.

The experimental UV profile of the volatile-rich material has been demonstrated to reproduce the shape and position of an astronomical extinction feature observed in a carbon-rich post-AGB object (HD 44179, "Red Rectangle", data by Vijh *et al.* 2005). This is true down to wavelengths of about 180nm whereas the steep extinction rise at shorter wavelengths cannot be explained (Fig. 11). Especially, this rise is not likely to be due to scattering from grains, which according to our results is non-monotonous and always weaker than absorption in this spectral range (I. Llamas Jansa, PhD thesis 2006). Vijh *et al.* (2005) attribute the FUV rise to the ionization edge of aromatic molecules.

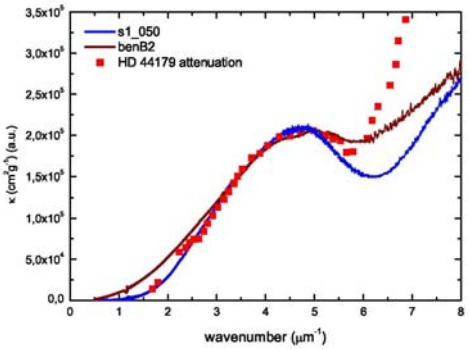

Fig. 11: Comparison of the UV extinction spectrum of the post-AGB object HD 44179 ("Red Rectangle") with those of the CAST soot produced at C/O=0.5 and with a pyrolysis product based on benzene precursor.

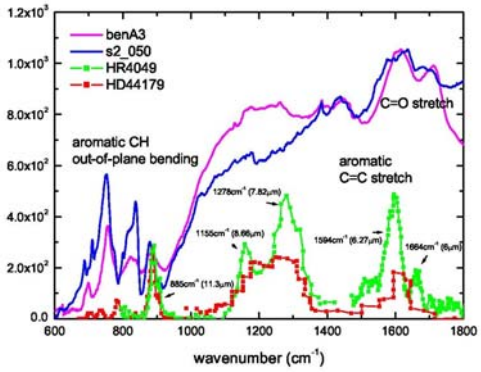

Fig. 12: Comparison of the IR emission spectra of the post-AGB objects HD 44179 ("Red Rectangle") and HR 4049 with those of the CAST soot produced at C/O=0.5 and with a pyrolysis product based on benzene

The infrared spectrum of our material unfortunately does not well reproduce the emission spectrum of the Red Rectangle which is entirely dominated by aromatic C-H and C=C bands. Although some of these bands are present in the experimental spectrum as well, our material is clearly stronger hydrogenated and possesses aliphatic components as well (Fig. 12). The same is true for pulsed-laser pyrolysis condensates from benzene. Note that the emission from HD 44179 originates from a different location within this object than the UV absorption spectrum, so that this does not contradict the possible presence of a material like our product in part of the object.

b) Products from cw laser pyrolysis

The carbon nanopowder samples were prepared by laser pyrolysis in collaboration with I. Voicu at the National Institute for Lasers, Plasma and Radiation Physics in Bucharest, Romania. The production of the PAH containing soot is described in detail in Jäger et al 2006. The addition of benzene to a precursor gas mixture of acetylene and ethylene increased the formation efficiency of PAHs in the soot materials considerably. In order to remove the soluble components from the soot sample quantitatively we used an extraction method such as soxleth extraction with toluene as the elution solvent. The toluene was removed by distillation. The extracts as well as the soot were characterized by different spectroscopic methods such as IR, UV/VIS and a combination of gas chromatographic and mass spectrometric (GC/MS) analyses.

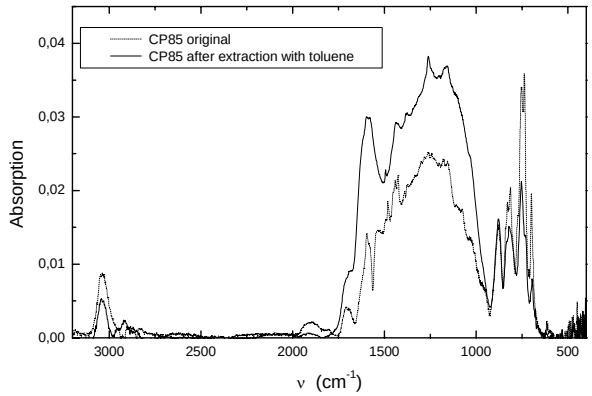

Fig. 13: Baseline corrected IR spectra of the soot sample before and after extraction of the PAH compounds.

The content of soluble components in the soot was determined to account for about 32% of the total soot mass. Interestingly, The PAHs can also be completely removed by heating the soot up to 350 °C in vacuum (10^{-5} mbar). The IR spectrum of the carbon nanopowder before and after extraction is shown in Fig. 15. The comparison of the spectra shows a partly disappearance or weakening of bands. First the intensity of the weak aromatic stretching vibration at 3050 cm^{-1} decreases by about 1/3. The intensity of the C=O band does not change in the extracted soot sample but disappears in annealed soot. The band at about 1600 cm^{-1} caused by C=C stretching vibrations becomes broader and stronger. However, the intensities and band profiles of the C-H out of plane vibrations between 700 and 900 cm^{-1} alter considerably. The first band at 879 cm^{-1} does not decrease its intensity, demonstrating that this band is completely originating in the soot structure. The two other features weaken extensively. Interestingly, the fourth band at 700 cm^{-1} is reduced by the half. This band is caused by 5 adjacent H atoms in an aromatic ring typical for compounds like biphenyl, triphenyl or triphenylbenzene.

The IR spectrum of the soluble soot component itself shows the presence of a variety of functional groups (Fig. 14). Bands between 3300 and 2800 cm^{-1} are caused by -C-H stretching vibrations of differently hybridized carbon. There are various aromatic =C-H bands between 3000 and 3100 cm^{-1}. These bands can originate from either a mixture of polycyclic aromatic compounds or the existence of substituents at the aromatic rings, which can influence the position of adjacent =C-H vibrational bands.

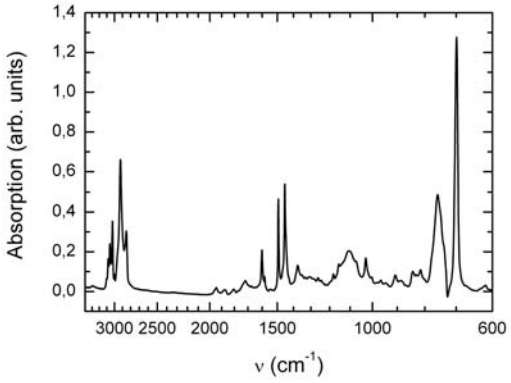

Fig. 14: IR absorption spectrum of the toluene extract measured at a film on a KBr substrate

The saturated -C-H stretching vibrations cause 2 strong bands at 2923 and 2853 cm^{-1} assigned to asymmetric and symmetric stretching vibrations of $–CH_2$ groups. Two weak shoulders at the short wavelength tail of these two bands can be attributed to the asymmetric and symmetric stretching vibrations of saturated -CH3 groups. Since the oscillator strength of the aromatic =C-H stretching vibration is about 5 times less than the oscillator strength of saturated -C-H, an overabundance of aromatic =C-H can be deduced. The strong dominance of saturated CH_2 compared to CH_3 groups is interesting. The dominance of the CH_2 groups results from the formation of dihydro-groups in the aromatic rings resulting in the destruction of the aromatic character of that ring and in the formation of compounds such as dihydro-cyclopentapyrene, dihydrobenzo-pyrene.

The features between 700 and 900 cm^{-1} due to out of plane vibrations of aromatic =C-H show the strongest IR band at 700 cm^{-1} which is already present in the soot spectrum before extraction (=C-H out of plane, 5 adjacent H atoms). There are two other strong bands at 731 and 756 cm^{-1} typical for 4 and 3 adjacent H atoms. Two weak bands between 800 and 850 cm^{-1} show a minor presence of 3 and 2 H in the aromatic ring.

M/z	PAHs
152,154	biphenyl, ethylnaphthalene and biphenylene
178	phenanthrene, anthracene and methylene-fluorene.
202	pyrene,fluoranthene
204	anthrocyclobutene, dicyclobutabiphenylene
226	cyclopentapyrene
228	naphthacene, chrysene, triphenylene: coronene
230	dimethyl-, ethyl-fluoranthene, dihydrocyclopenta-pyrene
252	benz-ace-phenanthrylene, phenylanthracene, perylene, benzopyrene
254	binaphthalene, phenylanthracene, dihydrobenzopyrene, dihydrobenzo-fluoranthene
276	dibenzochrysene, indenopyrene
278	benzochrysene, dihydrobenzoperylene
300	coronene
302	dibenzonaphthacene, naphthochrysene

Table 2 List of PAHs detected by GC/MS with mass number.

The GC/MS analyses show a distribution of PAH masses m/z ranging from 152 to 530. A zoo of different PAH molecules could be identified with the corresponding mass spectra (see Table 2). The extracted PAH compounds were used for further spectroscopic measurements in the UV/VIS and IR region. A more detailed description of the measurements and results is given in Jäger *et al.* (2006 and 2007a).

We found that the optical properties of the soot can be influenced by the adsorbed PAHs but we have also observed the opposite effect. The position of the IR bands of PAHs can be affected by the soot which was proven by IR measurements of phenanthrene molecules adsorbed on soot particles measured at room temperature (Fig. 15). The two strong bands of phenanthrene due to b_1 vibrations (818.8 and 732.9 cm^{-1}) were found to be at nearly the same position like phenanthrene molecules at 10 K (812.8 and 735.0 cm^{-1}) (Hudgins and Sandford 1998). However, according to these authors the difference of the temperatures should cause a shift by -3 cm^{-1} which cannot be observed. The expected band shift is obviously compensated by an equal shift to larger wavenumbers which is caused by an electronic interaction of the p electron system of the PAH molecules with the rather electron-poor p bonds in bent graphene layers on the surface of the soot nanoparticles.

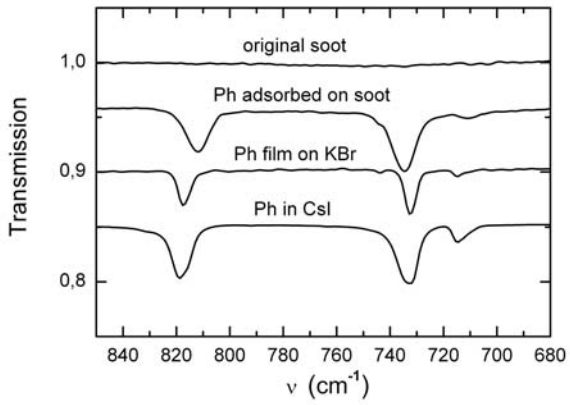

Fig. 15: IR spectrum of phenanthrene (Ph) adsorbed on carbon soot particles in comparison with spectra obtained from a phenanthrene film on KBr and from phenanthrene powder embedded in CsJ.

3.5.5. Investigation of the carbon grain formation process in gas-phase condensation

The high power densities of $2x10^8$-$9x10^9$ W/cm^2 due to the use of a pulsed laser in the laser ablation condensation experiments lead to high temperatures in the reaction and condensation zone and the formation of fullerene-like soot. By using the particle beam extraction in the hot and dense condensation zone we were able to quench the first carbon seed particles in the original condensation state and to avoid further processing like coalescence of the seeds to larger structures.

The HRTEM images of the soot samples show a number of fullerene-like particles with sizes between 1-3 nm. The observed particles consist of more or less disturbed or elongated carbon cage structures. Fig. 16 shows some small grains which are built by differently sized carbon cages. Especially interesting is the finding of parts of cage structures which are not closed completely. Such structures can be observed in Fig. 18. The right panel of this figure shows a bowl-like structure.

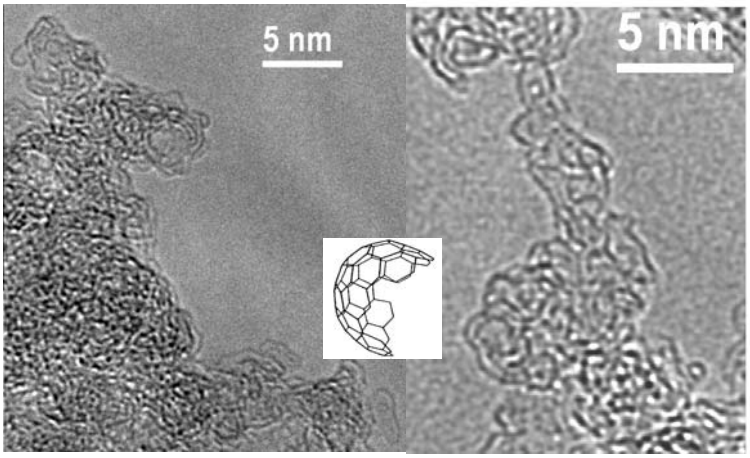

Fig. 16 HRTEM bright field images of small fullerene-like grains showing elongated fullerene structures and carbon cages. In the right panel one can observe an example of an incomplete cage structure (upper left corner).

The detection of these structures and the additional occurrence of ≡C-H bands of sp-hybridized carbon point to a particle formation process starting with C polyyne chains. These chains form finally saucer-shaped carbon structures which can combine to fullerene-like particles. This soot formation process is similar to a fullerene condensation process proposed by Kroto and McCay (1988). The side product or soluble components in these condensates are fullerenes. Laser pyrolysis of gas-phase hydrocarbons has been often used as an effective method to produce extractable components such as PAHs and fullerenes in condensed soots. Pope (1996) has calculated that the fullerene yield is at most for high temperatures and low pressures between 1800 and 2500 K. At temperatures lower than 1800 K, the side products are mainly PAHs, whereas at temperatures higher than 2500 K the pyrolysis products are composed of polyyne-based compounds.

Pulsed CO_2 laser pyrolysis of acetylene, ethylene and mixtures of both gases produces the same kind of very small fullerene-like carbon condensates (see Table 3). The power densities in the reaction zone which could be realized with the pulsed laser are between 10^7-10^9 W/cm^2 still preferring a high-temperature condensation process.

Precursor	Buffer gas	LP (W)	Laser	Power density W/cm^2	Side pro-ducts
C_2H_2, C_2H_4 SF_6	He	1-20	pulsed	$5x10^7$-$1x10^9$	fullerene-like soot
C_2H_4, C_6H_6	Ar	600	cw	5200	soot + PAHs (33wt%)
	Ar	850	cw	6500	soot + PAHs (17wt%)
C_6H_6, SF_6	Ar	60	cw	900	**100% PAHs (no soot)**

Table 3 Laser pyrolysis experiments used to condense carbon soot with different structures and soluble components.

The application of a cw laser with much less power density between 5200 and 6500 W/cm^2 provides a completely different condensate. The soot grains are rather large showing longer and less disturbed grapheme layers. The produced soot materials contain a remarkable amount of soluble components which turned out to consist of a mixture of plane PAH molecules (see next section). Here, the soot formation process is different compared to the high energy condensations. The lower the power density the higher is the content of PAHs. The decrease of the power density in the reaction zone reduces the amount of insoluble carbon soot grains. For a 60 W cw-CO_2 laser corresponding to a power density of 900 W/cm^2 only a soluble condensate was produced consisting of a mixture of PAHs. The soot condensation process is driven by a combination of small molecules, C_2 addition, formation of plane PAHs and subsequent condensation and growth of carbon grains, a formation scheme described by Richter and Howard (2000).

3.6 Zusammenfassung und Ausblick / Summary and future

We have investigated the structural and spectroscopic properties of carbonaceous condensates from various processes in a comprehensive way including co-condensation of carbides, different precursors, temperatures and reactive atmospheres. The results obtained allowed to draw conclusions about the incorporation of hydrogen and the condensation processes at high and low temperatures. The spectra measured agree partly with astronomical spectra of circumstellar carbon condensates. A strong UV resonance has been found with material rich in volatiles, the position of which, however, is different from the one of the interstellar UV hump. Furthermore, our investigation of the UV spectral properties of nano-diamonds from primitive meteorites (Mutschke *et al.* 2004) has led to a collaboration on the UV extinction in Active Galactic Nuclei (Binette *et al.* 2005, 2006)

We will continue this research in two directions. First, we intend to investigate the influence of UV irradiation on carbon structures and their UV spectra. According to Mennella *et al.* (1998) this has a crucial influence on the UV properties, but only a single experimental study is available for this so far. Second, we plan to intensify the investigation of volatile components from soot including a separation of the molecular species and their spectroscopic measurement.

3.7 Literatur / References

Allain, T., Sedlmayr, E., Leach, S., PAHs in circumstellar envelopes I. Processes affecting PAH formation and growth, Astron. Astrophys., **323** (1997), p. 163

Binette, L., Magris C., G., Krongold, Y., Morisset, C., Haro-Corzo, S., Antonio de Diego, J., Mutschke, H., Andersen, A.C.: *Nanodiamond dust and the far-ultraviolet quasar break,* Astrophys. J., **631** (2005) 661.

Binette, L., Andersen, A.C., Mutschke, H., Haro-Corzo, S.: *Nanodiamond dust and the energy distribution of quasars,* Astron. Nachr. **327** (2006) 151.

Bogana, M., Ravagnan, L., Casari, C.S., *et al.*: *Leaving the fullerene road: presence and stability of sp chains in sp2 carbon clusters and cluster-assembled solids,* New Journal of Physics **7** (2005) 81

Chhowalla, M., Wang, H., Sano, N., *et al.*: *Carbon Onions: Carriers of the 217.5nm Interstellar Absorption Feature,* Phys. Rev. Lett. **90** (2003) 155504.

Chigai, T., Yamamoto, T.,: *Condensation sequence of SiC and graphite grains around carbon stars,* Geochim. Cosmochim. Acta **67** (2003) Suppl. 1, A64.

Clayton, D.D., Deneault, E.A.N. and Meyer, B.S.: *Condensation of carbon in radioactive supernova gas*, Astrophys. J. **562** (2001) 480.

Duley, W.W., and Seahra, S.S.: *2175 Å and 3.4 Micron Absorption Bands and Carbon Depletion in the Diffuse Interstellar Medium,* Astrophys. J. **522** (1999), L129

Duley, W.W. and Lazarev, S.: *Ultraviolet absorption in amorphous carbons: PAHs and the 2175 Å extinction feature,* Astrophys. J. **612** (2004), L33.

Galvez, A., Herlin-Boime, N., Reynaud, C., Clinard, C., Rouzaud, J.N. : *Carbon nanoparticles from laser pyrolysis,* Carbon **40** (2002) 2775.

Hudgins, D., Sandford, S., J. Phys. Chem. A **102** (1998) 329

Iglesias-Groth, S.: *Fullerenes and buckyonions in the interstellar medium,* Astrophys. J. **608** (2004), L37.

Jäger, C., Krasnokutski, S., Staicu, A., Huisken, F., Mutschke, H., Henning, Th., Poppitz, W., Voicu, I.: *Identification and spectral properties of PAHs in carbonaceous soot produced by laser pyrolysis,* Astrophys. J. Suppl. Ser. **166** (2006) 557 .

Jäger, C., Mutschke, H., Huisken, F., Henning, Th., Voicu, I., Poppitz, W.: *Spectral characterization of soot by-products obtained by CO_2 laser pyrolysis of benzene/hydrocarbon vapors*, Phys. Chem. Chem. Phys. (2007a) in preparation

Jäger, C., Mutschke, H., Henning, Th., *Spectral and structural properties of carbon nanoparticles produced by laser ablation,* Astrophys. J., (2007b), in preparation.

Keller, A., Kovacs, R. and Homann, K.-H.: *Large molecules, ions, radicals and small soot particles in fuel-rich hydrocarbon flames,* Phys. Chem. Chem. Phys. **2** (2000) 1667.

Kwok, S., Volk, K., and Bernath, P.: *On the origin of infrared plateau features in proto-planetary nebulae*, Astrophys. J. **554** (2001), L87

Kroto, H.W., McKay K.: *The formation of quasi-icosahedral spiral shell carbon particles,* Nature **331** (1988) 328.

Llamas Jansa, I., Jäger, C., Mutschke, H., Henning, Th*.: Far-ultraviolet to near-infrared optical properties of carbon nanoparticles produced by pulsed-laser pyrolysis of hydrocarbons and their relation with structural variations*, Carbon, (2007), submitted

Llamas Jansa, I.: *Experimental study on the optical and structural properties of carbon nanoparticles.* Ph. D. Thesis, Friedrich Schiller Universität Jena, (2006)

Llamas Jansa, I.: *Spectroscopy and Structural Characterization of Carbon Nanoparticles Produced by Laser Pyrolysis of Acetylene*, Master Thesis (2002), Friedrich-Schiller-Universität Jena

Llamas Jansa, I., Mutschke, H., Clément D., Jäger, C., Henning, Th.: *IR spectroscopy of carbon nanoparticles from laser-induced gas pyrolysis*, In: Exploring the ISO Data Archive-Infrared Astronomy in the Internet Age, ed. C. Gry *et al.*, ESA SP-511 (2003) 69.

Lodders, K., Fegley Jr., B.: *Condensation chemistry of circumstellar grains*, In: Asymptptic Giant Branch Stars, ed. T. Le Bertre *et al.*, IAU Symp. **191** (1999) 279.

Mennella, V., Colangeli, L., Bussoletti, E., Palumbo, P., Rotundi, A.: *A new approach to the puzzle of the ultraviolet interstellar extinction bump*, Astrophys. J. **507** (1998) L177.

Mutschke, H., Andersen, A.C., Jäger, C., Henning, Th., Braatz, A.: *Optical data of meteoritic nano-diamonds from far-ultraviolet to far-infrared wavelengths,* Astron. Astrophys. **423** (2004) 983.

Palotas, A.B., Rainey, L.C., Feldermann, C.J., Sarofim, A.F., Vander Sande, J.B.: *Soot morphology: An application of image analysis in high-resolution transmission electron microscopy.* Microscopy Research and Technique **33** (1996) 266.

Peeters, E., Hony, S., Van Kerckhoven, C., *et al.*: *The rich 6 to 9 μm features of interstellar PAHs*, Astron. Astrophys. **390** (2002), 1089

Pendleton, Y.J. and Allamandola, L.J.: *The organic refractory material in the diffuse interstellar medium: Mid-infrared spectroscopic constraints*, Astrophys. J. Suppl. Ser. **138** (2002) 75.

Pope, C.J., Howard, J.B.: *Thermodynamic limitations for fullerene formation in flames,* Tetrahedron **52** (1996) 5161.

Reynaud, C., Guillois, O., Herlin-Boime, N., *et al.*: *Optical properties of synthetic carbon nanoparticles as model of cosmic dust*, Spectrochim. Acta Part A **57** (2001), 797

Robertson,J. and O'Reilly, E.P., *Electronic and atomic structure of amorphous carbon*, Physical Review **B 35** (1987), 2946

Schnaiter, M., Mutschke, H., Dorschner, J., Henning, Th., and Salama, F.: *Matrix-isolated nano-sized carbon grains as analog for the 217.5 nanometer feature carrier*, ApJ, Vol. 498 (1998), p. 486

Schnaiter, M., Gimmler, M., Linke, C., Jäger, C., Llamas Jansa, I., and Mutschke, H.: *Strong spectral dependence of light absorption by organic particles formed by propane combustion,* Atmospheric Chemistry and Physics Discussions, **6** (2006) 1841.

Stadermann, F.J., Croat, T.K., Bernatowicz, T.J., Amari, S., Messenger, S., Walker, R.M., Zinner, E.: *Supernova graphite in the NanoSIMS: Carbon, oxygen and titanium isotopic compositions of a spherule and its TiC sub-components,* Geochimica et Cosmochimica Acta, **69** (2005) 177.

Tomita, S., Fujii, M., Hayashi, S.: *Detective carbon onions in interstellar space as the origin of the optical extinction bump at 217.5 nm,* Astrophys. J. **609** (2004) 220.

Van Kerckhoven, C., Tielens, A.G.G.M. and Waelkens, C.: *Nanodiamonds around HD 97048 and Elias 1*, Astron. Astrophys. **384** (2002) 568.

Vijh, U.P., Witt, A.N. and Gordon, K.D.: *Blue Luminescence and the Presence of Small Polycyclic Aromatic Hydrocarbons in the Interstellar Medium,* Astrophys. J. **619** (2005) 368.

Witanachchi, S., Miyawa, A.M. and Mukherjee, P.: *Highly ionized carbon plasma generation by dual-laser ablation for diamond-like carbon film growth,* Mat. Res. Soc. Symp. **617** (2000) J3.6.1

Zubko, V.G., Mennella, V., Colangeli, L., and Bussoletti, E.: *Optical constants of cosmic carbon analogue grains-I. Simulation of clustering by a modified continuous distribution of ellipsoids,* Mon. Not. R. Astron. Soc. **282** (1996) 1321.